

Growth of ^3He crystals at different magnetic fields

J. Bueno¹, R. Blaauwgeers², A.Y. Parshin³, and R. Jochemsen⁴

¹ *Department of Physics, University of California, San Diego, 9500 Gilman Drive, La Jolla, CA 92093, USA*

² *Helsinki University of Technology, P.O. Box 2200, FIN — 02015 HUT, Finland*

³ *P.L. Kapitza Institute, 2 Kosygina Str., Moscow 119334, Russia*

⁴ *Kamerlingh Onnes Laboratory, LION, Leiden University, P.O. Box 9504, 2300 RA Leiden, The Netherlands*
E-mail: jochemsen@physics.leidenuniv.nl

Received November 16, 2007

The experiments on ^3He crystal growth are carried out in magnetic field up to 9 T. The data were analyzed and compared with the results found at zero magnetic field. It was found that the interface and the crystal lattice couple weakly in the presence of an external magnetic field, and we could set an upper limit of the step energy of the $\langle 110 \rangle$, $\langle 100 \rangle$ and $\langle 211 \rangle$ facets at different magnetic fields.

PACS: 73.43.Nq Quantum phase transitions;
75.30.Kz Magnetic phase boundaries (including magnetic transitions, metamagnetism, etc.).

Keywords: ^3He crystal, magnetic field, mechanisms of crystal growth.

1. Introduction

Last years there is a considerable interest to the problem of a growth of ^3He crystals. For example, recent experiments on ^3He crystal growth at zero magnetic field by Tsepelin et al. [1,2] revealed many facets and strong anisotropy in the growth rates. The problem of crystal growth in the presence of magnetic field is especially attractive because ^3He presents the unique superfluid ordered phases.

^3He presents a rich phase diagram, both in the liquid and solid state, in the presence of an external magnetic field. The complicated broken symmetry state characterizing the superfluidity leads to the existence of several different superfluid phases. When liquid ^3He is cooled down and reaches a temperature of approximately 2.5 mK at zero magnetic field and melting pressure, it enters the superfluid A -phase. If it is cooled down further, the liquid undergoes the B -phase transition at about 1.9 mK. If an external magnetic field is applied, there is another superfluid phase appearing in between the normal and the A -phase, the so-called A_1 -phase [3].

On the other hand, when solid ^3He is cooled down at zero magnetic field, it undergoes a transition into a magnetically ordered state at $T_N = 0.93$ mK, the so-called Néel transition. From the paramagnetic phase it enters

into the so-called U2D2 phase. The U2D2 phase (or low-field phase) is an antiferromagnetic phase with two planes of spins pointing up and two planes of spins pointing down in sequence. When the magnetic field reaches 450 mT, the solid transforms from the U2D2 to the CNAF (canted normal antiferromagnetic) phase. The CNAF phase (or high-field phase) is a normal antiferromagnetic phase, but with the spins tilted towards the magnetic field direction, giving a significant magnetization.

In Fig. 1 the phase diagrams of liquid and solid ^3He are plotted one on top of the other. The region around 500 mT and $T < 1$ mK is especially interesting because two phase transitions take place, one in the solid, from the U2D2 phase to the CNAF phase, and another one in the liquid, from the superfluid B -phase to the superfluid A -phase. Crystals can be grown from the same phase of the liquid (B -phase) into two different phases in the solid (U2D2 and CNAF), and from the two different superfluid phases (A -phase and B -phase) into the CNAF solid phase. This gives the possibility of determining the influence of the properties of both liquid and solid on the growth process.

The aim of present work is detailed experimental study of crystal growth in ^3He in wide range of magnetic field up to 9 T.

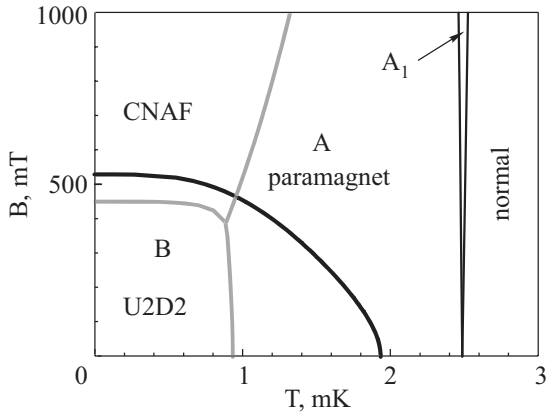


Fig. 1. Phase diagrams of liquid and solid ^3He in equilibrium at melting pressure in presence of an external magnetic field drawn in the same figure. Black lines denote the phase transition lines between the four liquid phases (the normal, A_1 , A - and B -phases). Grey lines indicate the phase transition lines in the solid at the same pressure, with the paramagnetic and the two ordered antiferromagnetic phases (U2D2 and CNAF).

2. Growth velocity of facets

Growing a crystal means that atoms from the liquid have to attach to nucleation sites in the solid. In order to grow a crystal a driving force needs to be applied. This driving force is the difference in the chemical potential between the liquid and the solid, which consists of two terms. One is due to the difference in temperature between the solid and the liquid and the other one is due to the applied overpressure (the deviation from the equilibrium melting pressure)

$$\Delta\mu = \Delta\mu_P + \Delta\mu_T. \quad (1)$$

In the temperature region of the experiments (between T_N and $0.5T_N$), the liquid is in the superfluid state while the crystal is grown, the heat generated at the interface is rapidly taken away by the liquid, allowing the solid and the liquid to be in thermal equilibrium. Therefore, the temperature difference driving force term can be neglected. The driving force will depend only on the externally applied overpressure to induce the growth of the crystal.

The effective growth coefficient k_{eff} , which is the measurable quantity, can be defined as [4]

$$k_{\text{eff}} = \frac{v_f}{\Delta\mu_P}, \quad (2)$$

where v_f is the velocity of the facet and $\Delta\mu_P$ is the chemical potential difference (per unit mass) between the liquid and the solid and can be expressed as

$$\Delta\mu_P = \left(\frac{\rho_s - \rho_l}{\rho_s \rho_l} \right) \Delta P \quad (3)$$

with ρ_s and ρ_l as the densities of the solid and liquid respectively, and ΔP the pressure change in the liquid with respect to the equilibrium melting pressure.

The effective growth coefficient has two contributions [5]. One term is due to bulk effects (bulk growth coefficient k_{bulk}) and takes into account the contribution due to the latent heat and the heat transport in the liquid and solid phases. This term strongly depends on the geometry of the experimental cell. The second term is due to the interface (intrinsic growth coefficient k_{int}), which in case of faceted growth is determined by spiral growth of elementary steps. So we write

$$\frac{1}{k_{\text{eff,growth}}} = \frac{1}{k_{\text{bulk,growth}}} + \frac{1}{k_{\text{int,growth}}}. \quad (4)$$

Note that the bulk term always lowers the growth coefficient. In the case of solid-superfluid ^3He , the bulk term can be expressed as [4]

$$\frac{1}{k_{\text{bulk,growth}}} = \frac{\rho_s}{T} Z_l L^2, \quad (5)$$

where Z_l is the thermal impedance of the liquid and L is the latent heat.

Since the latent heat vanishes very fast below the Néel transition, the bulk growth coefficient can be neglected. Thus, the effective growth coefficient gives a very good approximation of the intrinsic growth coefficient, which is the one which has all the physical information about the growth properties.

The effective melting coefficient can be defined as follows

$$\frac{1}{k_{\text{eff,melt}}} = \frac{1}{k_{\text{bulk,melt}}} + \frac{1}{k_{\text{int,melt}}}. \quad (6)$$

In general the bulk terms are equal $k_{\text{eff,growth}} = k_{\text{eff,melt}}$. We now define the ratio between $k_{\text{eff,growth}}$ and $k_{\text{eff,melt}}$ as

$$\eta = \frac{k_{\text{eff,growth}}}{k_{\text{eff,melt}}}. \quad (7)$$

Growing faceted interfaces is much slower than melting. Thus, if $\eta \ll 1$, meaning that melting is faster than growing, the bulk terms are negligible and the effective growth coefficient is actually the intrinsic one. A very extensive discussion about this problem can be found in the work by Akimoto *et al.* [6].

The velocity of a step moving on a facet can be expressed by

$$v_s = \mu d \left(\frac{\rho_s - \rho_l}{\rho_l} \right) \Delta P, \quad (8)$$

where μ is the step mobility, d is the height of the elementary step of the facet, ρ_s and ρ_l are the molar densities of solid and liquid ^3He respectively, and ΔP is the applied overpressure.

In the presence of screw dislocations, spiral growth is the main growth mechanism at low temperatures. The velocity of a facet can be expressed in the following way [2]

$$v_f = \frac{\mu d^3}{19\beta} \left(\frac{\rho_s - \rho_l}{\rho_l} \right)^2 K (\Delta P)^2, \quad (9)$$

where β is the step energy and K is the number of steps produced by one dislocation. Generally speaking, K depends on the Burgers vector of the dislocation, and in the simplest case $K = 1$. In absence of reliable data on characteristics of dislocations in our crystals we assume in the following $K = 1$, in correspondence with Ref. 7.

The step mobility has not yet been measured in ^3He . Below the Néel transition, the step mobility can be estimated by taking into account the two main processes which contribute to the step resistivity $1/\mu$, being the scattering of the magnons in the solid with the moving step and the scattering of the quasiparticles in the superfluid with the moving step.

Equation (9) predicts a quadratic dependence of the facet velocity on the applied overpressure. This behavior was not seen in the experiments of Tsepelin *et al.* [2], which are consistent with a linear behavior. This was explained as follows: If the step velocity increases to a certain critical velocity v_c at which Cherenkov-type creation of excitations occurs, the step mobility suddenly decreases. Then the growth velocity is not defined by Eq. (9), because in this regime the step velocity does not depend on the step mobility anymore and the facet velocity becomes linearly dependent on the overpressure ΔP . The expression for the facet growth velocity then becomes [2]

$$v_f = \frac{v_c d^2}{2\pi\beta} \left(\frac{\rho_s - \rho_l}{\rho_l} \right) \Delta P. \quad (10)$$

From Eq. (8) one can estimate the overpressure at which the facet velocity goes from a quadratic to a linear behavior. At that point the step velocity equals the critical velocity. If we assume that the critical velocity is given by the magnon velocity ($c = 8$ cm/s), and the mobility of the step is considered to be the one for magnon scattering [2], we get

$$d \left(\frac{\rho_s - \rho_l}{\rho_l} \right) (\Delta P)_c = \frac{v_s}{\mu} = \frac{c}{\mu_m} = \frac{(k_B T)^4 d^2}{w \hbar^3 c^3}. \quad (11)$$

This yields an overpressure of approximately 100 μbar . Below this value of the overpressure, the facet velocity may have a quadratic behavior (Eq. (9)), but

above it, the facet velocity depends linearly on the applied overpressure (Eq. (10)).

For magnons a rather low mobility of the step on the interface of the solid lattice is expected since the moving step directly touches and interacts with the spins close to the interface. For quasiparticles the coupling becomes significant only at higher step velocities [7], due to their large momentum and the large value of the effective width w of the step.

3. Experimental techniques

Nucleating a single ^3He crystal is not a very simple operation. Since the slope in the ^3He melting curve is negative at low temperatures, the crystal nucleates at the warmest spot in the cell. Once the crystal is nucleated and has grown for a while, this is not the warmest spot in the cell anymore, since the growth of the crystal locally cools the liquid (Pomeranchuk effect). Therefore, a second crystal may nucleate at the new warmest spot of the cell. Nevertheless, for temperatures below the Néel transition (our region of interest), where the latent heat is almost zero and the liquid is superfluid, the nucleation is relatively easy. The procedure is as follows. First, all the solid ^3He in the experimental cell is melted until there is only liquid in the cell. The ^3He is then slowly pressurized with a constant mass flow increasing the pressure in the ^4He side of the Pomeranchuk cell. When the ^3He pressure is just above the melting pressure (about 1 mbar) but still without solid nucleated, a heat pulse of 2.5 nW for 2–3 s is applied to the liquid at the bottom of the cell inducing nucleation of solid, indicated by the sharp drop of the ^3He pressure. Once the crystal has been nucleated, it continues to grow at (more or less) constant overpressure for inspection. After this, the crystal is melted till a smooth round seed is left ready for accurate growth and melting sequences.

The velocities of different facets were measured for several crystals as a function of the applied overpressure at a few values of the magnetic field.

The optical system is basically the one developed by Marchenkov *et al.* [8,9], but with some modifications described by Blaauwgeers *et al.* [10].

At present the light comes from outside into the cryostat through a 200 μm multimode optical fiber. The light is directed through the pure quartz windows in the optical part of our experimental cell [10] and it is focused with three lenses on the CCD camera placed in the inner vacuum can.

Once two-dimensional images of the crystals have been taken in the experiment, the next aim is to reconstruct the three-dimensional crystal shape. For this reconstruction additional information about the object is needed, like knowledge about the crystal structure. It is known that ^3He crystallizes in the bcc structure and

therefore the angles between the different facets are known.

An interactive computer program has been developed, which allows the user to analyze pictures of crystals having facets with the $\langle 110 \rangle$, $\langle 100 \rangle$ and $\langle 211 \rangle$ orientation. The working principles of this program are described in the work by Dekker *et al.* [11].

The analysis of a particular crystal can be followed in Fig. 2. First, a bitmap image of the ^3He is loaded and a calculated 2D projection of a bcc faceted crystal is drawn on the screen and placed on top of the image (Fig. 2,a). The model crystal can be rotated along its own axes and along the optical axis and it can be translated over the screen vertically and horizontally. Facets can be placed further from or closer to the origin of the crystal and different types of facets can be included or excluded. The simulation process takes place on the screen. Obviously, the user makes the first guess about the orientation of the crystal axes. On the basis of the bcc structure, an educated guess is made to assign certain Miller indices to a particular observed facet. The program provides an interactive trial and error method to fit the wire-frame to the image of the crystal (Fig. 2,b). Once the measured image is perfectly fitted by the calculated wire-frame, another image of the crystal (after a few minutes of growth) is uploaded into the program (Fig. 2,c). In the analysis of this new picture, the origin and the orientation of the computed crystal with the fitted wire-frame are kept the same, but the length from the origin to each facet is changed until the crystal image is again perfectly fitted (Fig. 2,d). The length change of the normal vector to each facet will be a quantity in pixels and, as the real-space dimensions of the image are known, the velocity of each facet can be determined by the pixel/real-space ratio.

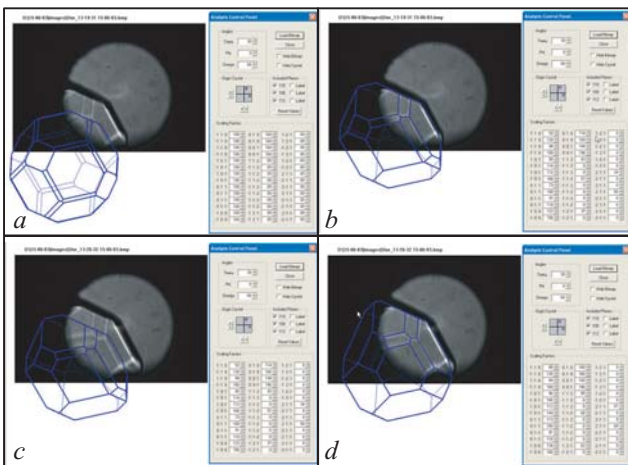


Fig. 2. This figure shows the computer program [11] that generates a wireframe of a bcc crystal and how it is used for the analysis of the data.

Nevertheless, there is a fundamental uncertainty in the program inherent to the process of making a projection of the crystal. Namely, the 2D projection image does not change if each facet of the real crystal would move by $v \cos \phi_i \Delta t$, where ϕ_i is the angle between the normal to the i -facet and the optical axis z . Such a process would correspond to the shift of the whole crystal by $v \Delta t$ along z (see Fig. 3). This degree of freedom is out of control of the method used. It means that a term $v \cos \phi_i$ may be added to the measured velocity of each facet without further change of the wire-frame image, and the value of v is only limited by the condition that the total velocity of each facet is positive.

An extra assumption is therefore needed. It is reasonable to assume that facets of the same type are growing with the same velocity. Then the «optical axis» contribution can be determined unambiguously, provided that at least two different facets of the same type but with different $\cos \phi_i$ are present in the crystal image. Moreover, this assumption can be checked directly if more than two such facets are present.

All crystals were analyzed with and without this assumption. Most of them showed a difference in velocity lower than 10%. There were only few crystals which velocities were dramatically different after applying this assumption. These crystals were not used in the following discussion. Therefore, the assumption that for a given crystal all facets of a given type grow with the same velocity is valid for data presented in this paper.

Once the velocity of each facet is known, only the applied overpressure for growing the crystal needs to be determined to obtain the growth coefficient.

When the solid/liquid system is in equilibrium, that is without growing or melting, it is at the equilibrium melting pressure. When the crystal is being grown (or melted), the pressure is different from the equilibrium melting pressure. The pressure difference is the driving force for the growth (or melting) process, and it is called the overpressure (or underpressure).

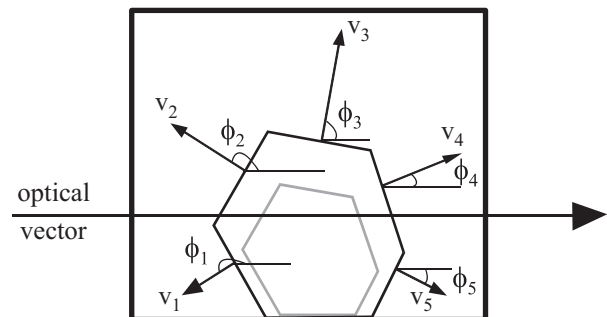


Fig. 3. Scheme illustrating the fundamental uncertainty of the data analysis. See text for details.

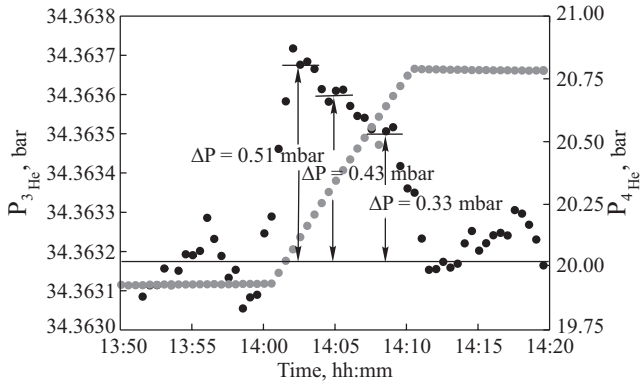


Fig. 4. The applied overpressure for growing the crystal is obtained from the melting pressure. Black points correspond to the ^3He pressure and grey points to the ^4He pressure. This crystal was grown at zero magnetic field and a temperature of 0.65 mK. See text for details.

As can be seen in Fig. 4, during the same growth experiment, different overpressures were obtained. Each of these overpressures corresponds to a different growth velocity. Thus, in the same growth sequence, different overpressures and velocities were obtained.

It is also interesting to know that if there is only one crystal present in the experimental cell. The amount of solid, or the solid fraction, can be calculated with the following expression [12]

$$x_s = \frac{v_l}{\Delta v_{sl}} [(\alpha + \kappa)(P_3 - P_{3m}) - \alpha(P_4 - P_{4m})], \quad (12)$$

where P_3 and P_4 are the ^3He and ^4He pressures respectively (see Fig. 11), v_l is the liquid molar volume at the pressure P_3 , Δv_{sl} is the difference between molar volumes of the liquid and the solid, $\kappa = \kappa_l \simeq \kappa_s$ is the compress-

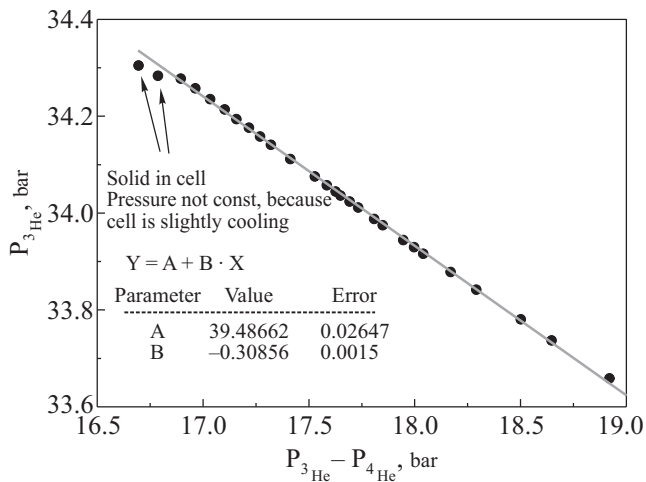


Fig. 5. Performance of the experimental Pomeranchuk cell during a compression. Note that the slope of $P_{3\text{He}}$ abruptly changes when solid is nucleated. The elasticity of the cell is obtained from the slope of the fit.

ibility of liquid (solid) ^3He and P_{3m} and P_{4m} are the ^3He and ^4He pressures when the solid is nucleated. The elasticity of the cell α is obtained from the slope of P_3 versus $P_3 - P_4$ during the compression in the all-liquid state (see Fig. 5). The solid fraction was calculated for each crystal grown in our experiments showing that the amount of solid in the cell was around 1% at the end of each growth. The volume of the crystal seen in the optical view can be estimated since the light beam had a diameter of 3.5–4 mm. Calculating the ratio between the volume of the crystal with the volume of the cell and comparing it with the solid fraction, it can be concluded that there was only one crystal present in the cell during each growth sequence.

4. Experiments at $B = 0$ T

In this section the experiments carried out at zero magnetic field and a temperature of 0.65 mK are described. At zero magnetic field, the liquid is in the superfluid B -phase and the solid is magnetically ordered in the U2D2 phase.

Since the experimental cell was cooled down for the first time, the main aim of the experiments at zero magnetic field was to check whether it was possible to cool ^3He down below the Néel transition and grow crystals at these temperatures, as well as to compare the results with the measurements by Tsepelin *et al.* [2,7].

In these experiments only the $\langle 110 \rangle$ and $\langle 100 \rangle$ facets were seen while Tsepelin *et al.* [2] have seen up to eleven different facets. In previous experiments in Leiden by Wagner *et al.* [13] also the $\langle 211 \rangle$ facet was seen. The reason for this significant difference in the amount of different types of facets might be the different analyzing techniques. While in Leiden direct images of the crystals are used, Tsepelin *et al.* used an interferometer in the cryostat and the phase shift technique, obtaining a higher sensitivity [14].

The same seed was kept for one day, growing faceted crystals and melting them several times per day.

A typical growth of a crystal is shown in Fig. 6. It was grown from an apparently smooth rounded seed and immediately after applying overpressure to the cell, the crystal started growing and got its faceted growth shape, since the temperature was far below the roughening temperature of many facet types. The slowest growing facets determined the shape of the crystal very quickly.

The results for the $\langle 110 \rangle$ and $\langle 100 \rangle$ facets are depicted in Fig. 7. Black points correspond to the $\langle 110 \rangle$ facet while the grey points correspond to the $\langle 100 \rangle$ facet.

Various slopes can be seen in Fig. 7. Part of the difference in the slopes may be explained in terms of the uncertainty in the measurement of the applied overpressure. In our experiment overpressures down to 0.1 mbar were measured. The pressure gauge had an accuracy of 0.05 mbar, which gave a considerable uncertainty in the

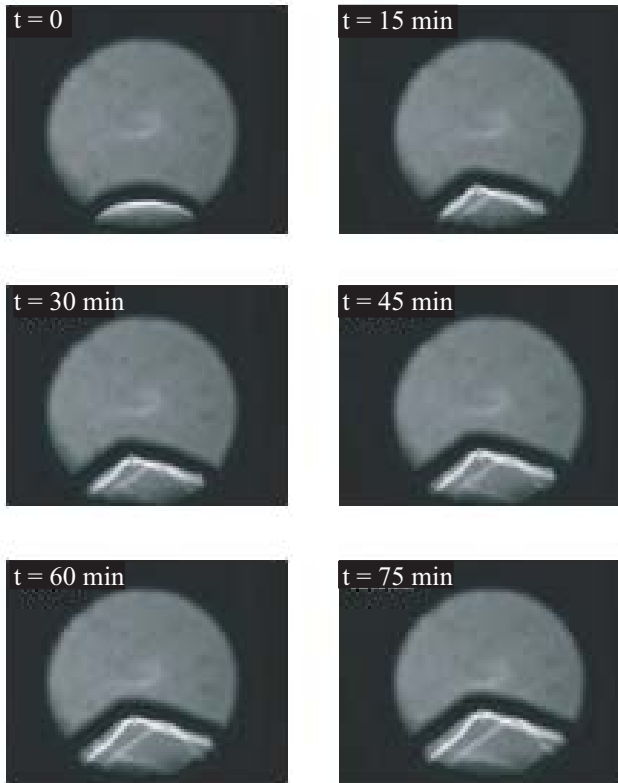


Fig. 6. Typical growth of a crystal at zero magnetic field. The diameter of the visible area is about 4 mm.

measurements. However, the difference in the facet velocities is too big for being only caused by an error in the measured applied overpressure. It might be possible that this difference is due to a real difference in the velocity of the same facet type.

The effective growth coefficient k_{eff} and the step energy β were calculated for each facet of each crystal, using

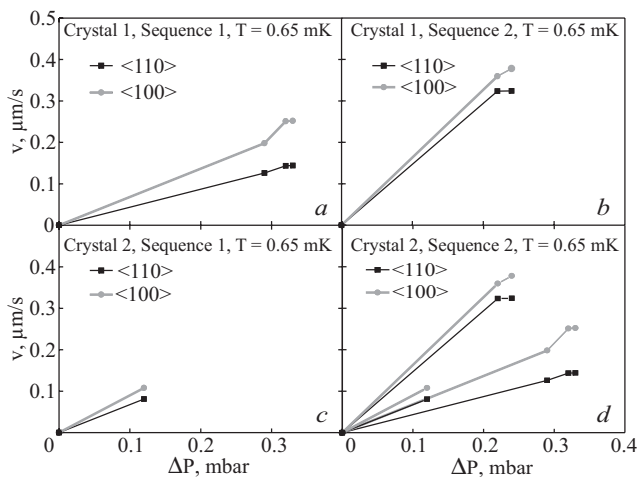


Fig. 7. Velocities of the different facets plotted versus the applied overpressure below the Néel transition at $B = 0$ T. Black points correspond to $\langle 110 \rangle$ facet and light grey to $\langle 100 \rangle$ facet. Solid lines connecting points are drawn to guide the eyes.

Eq. (2) and Eq. (10), and the results are shown in Table 1, in comparison with the step energies obtained by Tsepelin *et al.* [2].

Table 1. Effective growth coefficients (s/m) and step energies (erg/cm) for the different facets seen at zero magnetic field.

Facet	Crystal	k_{eff} (10^{-5})	β at $B = 0$ T (10^{-10})	
			This work	Tsepelin <i>et al.</i> [2]
$\langle 110 \rangle$	a	13 ± 0.4	11 ± 3	6.6
$\langle 110 \rangle$	b	4 ± 1	3.6 ± 0.9	
$\langle 110 \rangle$	c	2 ± 1	7 ± 3.5	
$\langle 100 \rangle$	a	23 ± 0.7	3 ± 1	1.6
$\langle 100 \rangle$	b	5 ± 2	14 ± 0.6	
$\langle 100 \rangle$	c	3 ± 2	2.4 ± 1.6	

The step energies measured by Tsepelin *et al.* [2] and the averaged value of the step energies found in this work ($\beta_{\langle 110 \rangle} = (7.2 \pm 2.5) \cdot 10^{-10}$ erg/cm, $\beta_{\langle 100 \rangle} = (2.3 \pm 1) \cdot 10^{-10}$ erg/cm) are in agreement with each other.

5. Experiments at $B = 2$ T

In this section the experiments carried out at a magnetic field of 2 T and at $T \approx 1$ mK are described. At this value of the magnetic field, the liquid is in the superfluid A-phase and the solid orders into the CNAF phase.

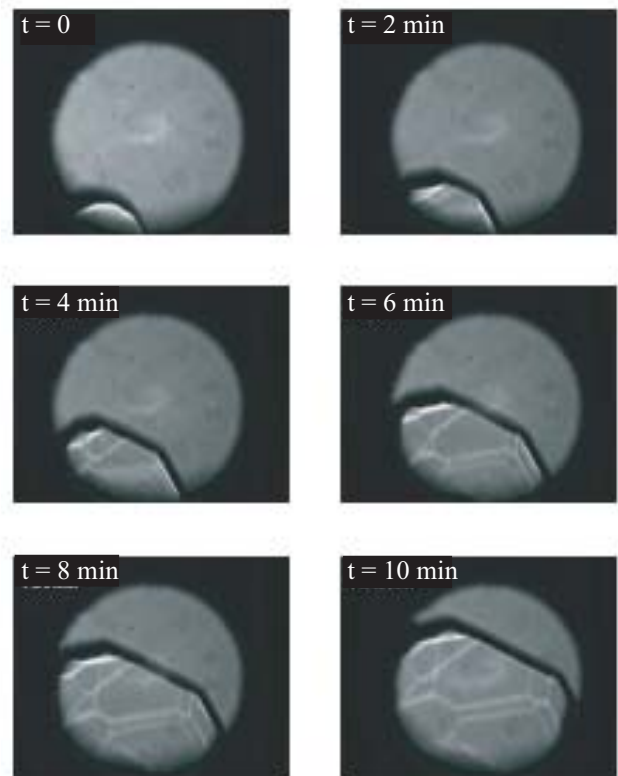


Fig. 8. Typical growth of a crystal at $B = 2$ T.

A typical growth process of a crystal at $B = 2$ T is shown in Fig. 8. It was grown from an apparently smooth rounded seed and immediately after applying overpressure to the cell, the crystal started growing and large facets became visible. Note that the shape of the faceted crystal seems different from the crystal grown at zero magnetic field in Fig. 6. Also remarkable is the significant change in the time it takes to grow a crystal of the same size. At $B = 2$ T more facets can be seen and the crystal grows much faster.

These crystals were analyzed as explained earlier. At this magnetic field value ($B = 2$ T) three different facet types were observed. Their velocities as function of the overpressure are shown in Fig. 9.

The first thing to notice is that the facet velocity has become larger for the $\langle 110 \rangle$ and $\langle 100 \rangle$ facets and that also the $\langle 211 \rangle$ facet type is now seen, while it was not observed at zero magnetic field.

The effect of the magnetic orientation with the applied magnetic field was checked in this set of measurements. If there is such a relation present in the crystal, it has to be larger for the $\langle 100 \rangle$ facet. The velocities of $\langle 100 \rangle$ facets of the same crystal, parallel and perpendicular to the external magnetic field were measured and compared. The growth rate for these facets (parallel and perpendicular) turned out to be same within a 10%.

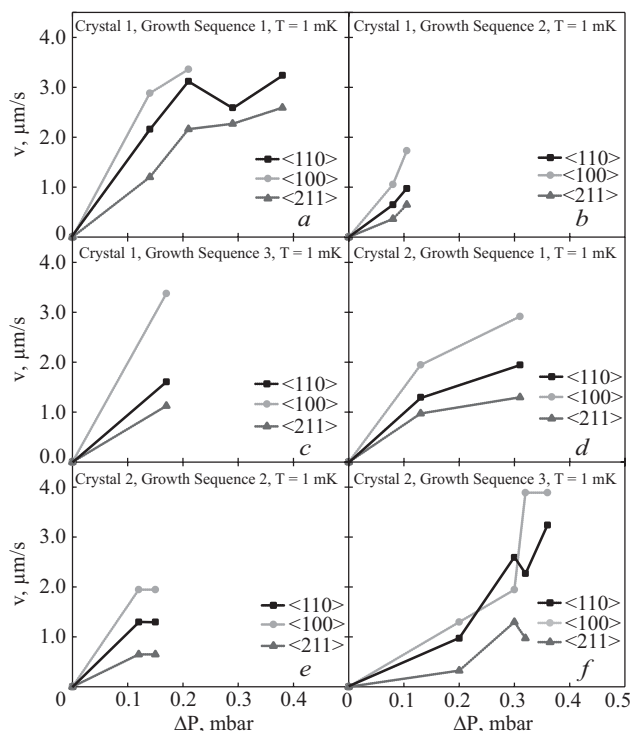


Fig. 9. Velocities of the different facets plotted versus the applied overpressure below the Néel transition at $B = 2$ T. Black points correspond to $\langle 110 \rangle$ facet, light grey to $\langle 100 \rangle$ facet and dark grey to $\langle 211 \rangle$ facet. Solid lines connecting points are drawn to guide the eyes.

It is also very surprising that the $\langle 110 \rangle$ is not the slowest facet anymore. The $\langle 110 \rangle$ facet is the slowest one in the absence of magnetic field. Since it has the largest interplanar distance, it was expected to be the most stable facet also in the presence of a magnetic field. Although the solid has a different magnetic order, still the crystal symmetry is roughly the same, so not such a big change was expected.

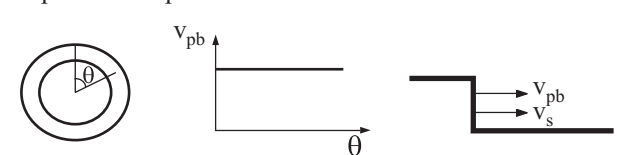
It might be thought that this inversion of growth rate for the two facet types could be due to the different liquid phase from which the solid grows. While at zero magnetic field the crystal is grown from the superfluid B -phase, at $B = 2$ T it is grown from the superfluid A -phase. The superfluid B -phase is isotropic in the k -space, resulting in an isotropic pair-breaking velocity. On the other hand, the superfluid A -phase has two nodes on the poles of the Fermi sphere, where the pair-breaking velocity goes to zero, with a maximum in the equator of the sphere [3].

It can be argued, however, that this anisotropy is not important in the present case. Indeed, a step moving at velocity v_s radiates excitations by the Cherenkov mechanism at an angle ϕ defined as $v_s \sin \phi = v_{pb} = \Delta(\theta)/p_f$, where p_f is the Fermi momentum (see Fig. 10). On the other hand, the energy gap Δ depends on the angle θ in k -space calculated from the vector \mathbf{l} as $\Delta = \Delta_0 \sin \theta$. As usual, we assume that \mathbf{l} is normal to the facet, which implies that $\phi = \theta$. We see that the critical velocity $v_{s,c}$ is still determined by Δ_0 for all excitations independent of the radiation angle.

Thus, a possible change in the facet velocity at the A transition could be due to the change of Δ_0 .

Since the magnon velocity in the solid [15] is still lower than the pair breaking velocity of the liquid ($v_{pb} \approx 10$ cm/s), the magnon velocity will be used as the critical velocity in the analysis. However, there is a cross-over of the magnon and pair breaking velocities around

Superfluid B-phase



Superfluid A-phase

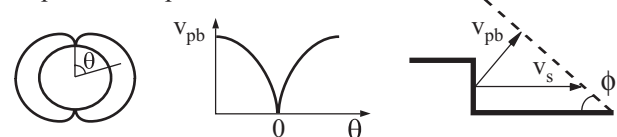


Fig. 10. Scheme of the pair breaking velocity for the superfluid A -phase. The superfluid B -phase is also shown for comparison. See text for details.

$B = 2.5$ T. Above this magnetic field, the magnon velocity becomes larger than the pair breaking velocity. Thus, for magnetic fields higher than $B = 2.5$ T the pair breaking velocity will be used as critical velocity in Eq. (10), while the magnon velocity will be used below this field.

The effective growth coefficient k_{eff} was determined for each facet of each crystal. The step energies of the different facets were deduced from the facet velocities with Eq. (10), using as a critical velocity the magnon velocity [15] ($v_c \simeq 8$ cm/s). These step energies are compared with the ones at zero field (see Table 2).

Table 2. Effective growth coefficients (s/m) and step energies (erg/cm) for the different facets seen at $B = 2$ T and compared with values found at zero magnetic field in this work and in the work by Tsepelin *et al.* [2]

Facet	Crystal	k_{eff} (10^{-5})	β at $B = 2$ T (10^{-10})	β at $B = 0$ T (10^{-10})
<110>	a	30 ± 12	0.5 ± 0.2	7.2 ± 2.5
<110>	b	26 ± 15	0.6 ± 0.3	
<110>	c	28 ± 13	0.5 ± 0.2	
<110>	d	20 ± 8	0.7 ± 0.3	
<110>	e	30 ± 22	0.5 ± 0.3	
<110>	f	23 ± 9	0.6 ± 0.2	
<100>	a	50 ± 12	0.14 ± 0.03	2.3 ± 1
<100>	b	45 ± 20	0.16 ± 0.07	
<100>	c	59 ± 17	0.12 ± 0.03	
<100>	d	30 ± 8	0.24 ± 0.06	
<100>	e	44 ± 20	0.16 ± 0.07	
<100>	f	30 ± 7	0.24 ± 0.06	
<211>	a	23 ± 6	0.21 ± 0.05	0.33 [2]
<211>	b	17 ± 9	0.3 ± 0.15	
<211>	c	20 ± 4	0.24 ± 0.05	
<211>	d	15 ± 4	0.32 ± 0.09	
<211>	e	15 ± 8	0.3 ± 0.15	
<211>	f	10 ± 3	0.5 ± 0.1	

If the analysis is done in terms of growth with critical step velocities, it would indicate that the averaged step energy at $B = 2$ T of the facets <110> ($\beta_{\langle 110 \rangle} = (0.57 \pm 0.25) \cdot 10^{-10}$ erg/cm) and <100> ($\beta_{\langle 100 \rangle} = (0.18 \pm 0.05) \cdot 10^{-10}$ erg/cm) is one order of magnitude smaller than at zero magnetic field, showing that the presence of an external magnetic field indeed affects the growth kinetics of the crystal. The consequences will be discussed later. On the other hand, the step energy of the

<211> ($\beta_{\langle 211 \rangle} = (0.3 \pm 0.1) \cdot 10^{-10}$ erg/cm) remains almost unaltered.

6. Experiments at $B = 8$ T

In this section the experiments carried out at a magnetic field of 8 T are described. At this field, the liquid is in the superfluid A_1 -phase and the solid orders into the CNAF phase. Some experiments were also carried out when the liquid was in the normal Fermi liquid state.

A typical growth of a crystal at $B = 8$ T is shown in Fig. 11. It was grown from an apparently smooth rounded seed and immediately after applying overpressure to the cell, the crystal started growing with large facets visible. Note that the shape of the crystal is different from the shape of the crystal grown at zero magnetic field in Fig. 6. Note also the difference in time it takes to grow a «large» crystal. At $B = 8$ T more facet types can be seen and the crystal grows much faster. The quality of these images is not as good as those taken at zero magnetic field and at $B = 2$ T since the optical access to the experimental cell got worse during the cool down.

At this magnetic field ($B = 8$ T) again three different types of facets were observed below the Néel transition ($T_N = 3.1$ mK) and in the superfluid A_1 -phase ($T_{A_1} = 2.7$ mK). The velocities for the three of them can be seen in Fig. 12.

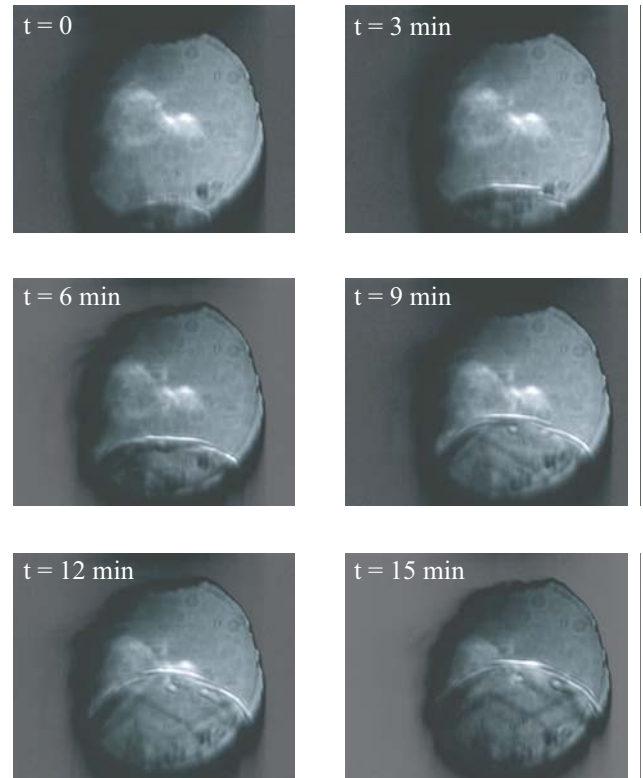


Fig. 11. Typical growth of a crystal at $B = 8$ T at $T = 2.5$ mK.

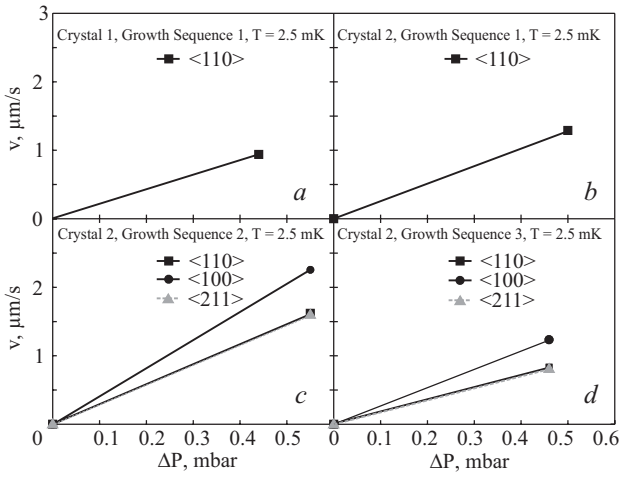


Fig. 12. Velocities of the different facets plotted versus the applied overpressure below the Néel transition of a crystals grown from the superfluid A_1 -phase at $B = 8$ T. Black point correspond to $\langle 110 \rangle$ facet, light grey to $\langle 100 \rangle$ facet and dark grey to $\langle 211 \rangle$ facet. Solid lines connecting points are drawn to guide the eyes.

The effective growth coefficient k_{eff} and the step energy β were calculated for each facet of each crystal and shown in Table 3. The step energies of the different facets seen during the experiment below the T_{A_1} transition were calculated using as the critical velocity the pair breaking velocity ($v_c \simeq 10$ cm/s). These step energies were compared with the ones obtained at zero magnetic field (see Table 3).

Table 3. Effective growth coefficients (s/m) and step energies (erg/cm) for the different facets seen at $B = 8$ T and compared with values found at zero magnetic field in this work and in the work by Tsepelin *et al.* [2].

Facet	Crystal	k_{eff} (10^{-5})	β at $B = 8$ T (10^{-10})	β at $B = 0$ T (10^{-10})
$\langle 110 \rangle$	a	6 ± 3	3 ± 1.5	7.2 ± 2.5
$\langle 110 \rangle$	b	8 ± 3	2.2 ± 0.8	
$\langle 110 \rangle$	c	9 ± 2	3.6 ± 0.8	
$\langle 110 \rangle$	d	5 ± 2	4 ± 1	
$\langle 100 \rangle$	c	12 ± 2	0.7 ± 0.1	2.3 ± 1
$\langle 100 \rangle$	d	8 ± 3	1.1 ± 0.4	
$\langle 211 \rangle$	c	9 ± 2	0.8 ± 0.2	0.33 [2]
$\langle 211 \rangle$	d	5 ± 2	1.2 ± 0.5	

The averaged step energies of each type of facet ($\beta_{\langle 110 \rangle} = (3 \pm 1) \cdot 10^{-10}$ erg/cm), $\beta_{\langle 100 \rangle} = (0.9 \pm 0.3) \cdot 10^{-10}$ erg/cm), $\beta_{\langle 211 \rangle} = (1 \pm 0.4) \cdot 10^{-10}$ erg/cm)) have increased compared with the step energies found at $B = 2$ T.

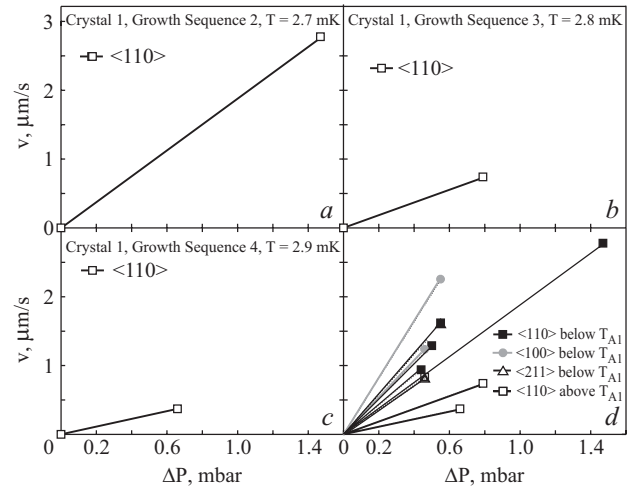


Fig. 13. Velocities of the different facets plotted versus the applied overpressure slightly above the superfluid transition at $B = 8$ T (a), (b), (c); the data below and above the superfluid transition (d). Black point correspond to $\langle 110 \rangle$ facet, light grey to $\langle 100 \rangle$ facet, dark grey to $\langle 211 \rangle$ facet and black open symbol for the $\langle 110 \rangle$ facet above the superfluid transition. Solid lines connecting points are drawn to guide the eyes.

The velocity of the $\langle 110 \rangle$ facet has been also measured below the Néel transition ($T_N = 3.1$ mK), but above the superfluid A_1 -phase ($T_{A_1} = 2.7$ mK), i.e. when the solid was growing from the Fermi liquid state. This experiment was performed while the cell was slowly warming up. No other types of facets were seen at these conditions. The $\langle 110 \rangle$ facet velocity was measured exactly at the superfluid transition ($T_{A_1} = 2.7$ mK) (see Fig. 13,a) and slightly above (Fig. 13,b at $T = 2.8$ mK and Fig. 13,c at $T = 2.9$ mK), showing some temperature dependence. In Fig. 13,d the velocities below and above the superfluid A_1 -phase transition are compared.

The difference in the $\langle 110 \rangle$ facet velocity below and above the superfluid transition is an indication that the liquid plays an important role in the growth mechanism.

The explanation for this observation might be that the heat generated at the interface by the growth of the crystal is no longer carried out as fast as when the liquid was in the superfluid phase, yielding to a local heating of the interface.

Another possible effect of growing crystals from the normal liquid phase may be that there are no spin currents in the liquid, making the attachment of the atoms from the liquid to the solid slower since the solid is magnetically oriented.

7. Preliminary Experiments at $B = 0.8$ T

Experiments at a magnetic field of 0.8 T at a temperature of approximately 1 mK were also done. At this field, the liquid is in the superfluid A -phase and the solid magnetically orders into the CNAF phase.

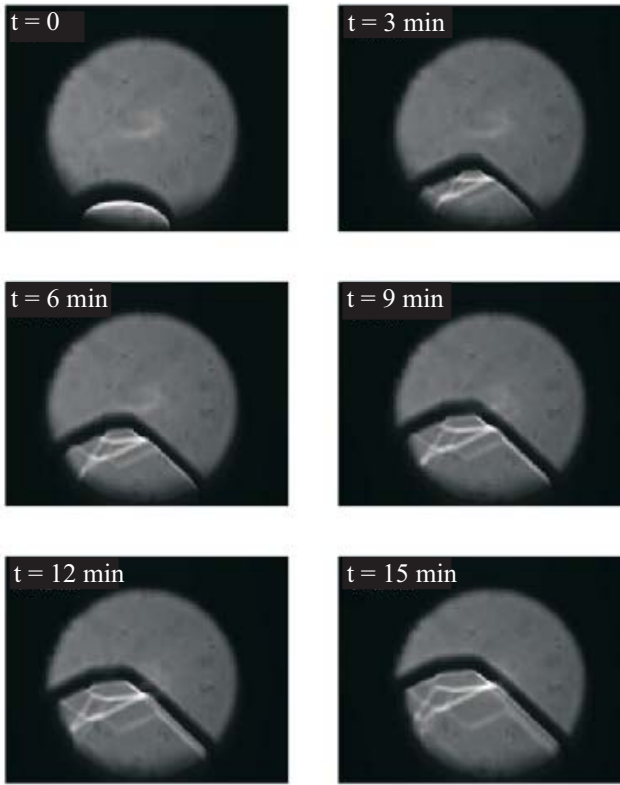


Fig. 14. Typical growth of a crystal at $B = 0.8$ T.

A typical growth sequence of a crystal at $B = 0.8$ T is shown in Fig. 14. As in the previous situations, it was grown from an apparently smooth rounded seed and immediately after applying overpressure to the cell, the crystal started growing while getting facets. More facets were seen compared to a crystal grown at zero magnetic field in Fig. 6. Notice as well that the crystal grows faster.

Since the magnon velocity in the solid at this magnetic field [16] is lower than the pair breaking velocity of the liquid ($v_{pb} \approx 10$ cm/s), the magnon velocity will be used as the critical velocity ($v_c \approx 5$ cm/s) in the analysis.

Unfortunately, the analysis of the data taken at this magnetic field turned out to be very difficult since it was very complicated to fit the crystals with the computer program. The computer program only generates $\langle 110 \rangle$, $\langle 100 \rangle$ and $\langle 211 \rangle$ facets. It might happen that more or different facets than the ones generated by the program were present in this crystal, making the fitting process impossible with the present version of our analysis program. Another possible reason might be the fact that only two adjacent $\langle 110 \rangle$ facets were seen in the crystal. In a normal fitting process, three adjacent $\langle 110 \rangle$ facets are needed to be completely sure that the assumption that *each* type of facet of a crystal is moving with the same velocity during the growth is valid. Somehow, this could also affect the fitting procedure. Nevertheless, an upper limit for the velocity of the $\langle 110 \rangle$ facet could be obtained.

The step energy of the $\langle 110 \rangle$ facet is compared with the one obtained at zero magnetic field in Table 4. Notice

that the step energy at $B = 0.8$ T of the $\langle 110 \rangle$ facet is almost one order of magnitude smaller than the one obtained by Tsepelin *et al.* [2] at zero magnetic field, confirming that the presence of an external magnetic field indeed affects their behavior as previously mentioned in Sec. 5.

Table 4. Upper limits for the value of the effective growth coefficient k_{eff} (s/m) and for the step energy β (erg/cm) for the $\langle 110 \rangle$ facet at $B = 0.8$ T.

Facet	k_{eff} (10^{-5})	β at $B = 0.8$ T (10^{-10})	β at $B = 0$ T (10^{-10})
$\langle 110 \rangle$	11 ± 5	0.81 ± 0.35	7.2 ± 2.5

8. Discussion

This section is a summary of the measurements taken on ^3He below the Néel transition, possible conclusions and open lines to continue these studies.

Crystals have been grown at different magnetic fields ($B = 0, 2, 8, 0.8$ T) below the Néel transition showing a significant anisotropy in the growth rates for the different facets. The growth rates can vary by more than one order of magnitude dependent on the value of the magnetic field.

The effective growth coefficient and the effective melting coefficient were calculated for various facets of different crystals at different conditions, as well as the ratio between both, η (see Eq. (7)). The value for η varies between 0.25 and 0.33, which means that melting was 3–4 times faster than growing. These values for η show that to a reasonable approximation we were measuring the intrinsic growth coefficient and not the bulk growth coefficient in our experiments.

The step energies of these crystals for different facets were calculated supposing high step mobility, which

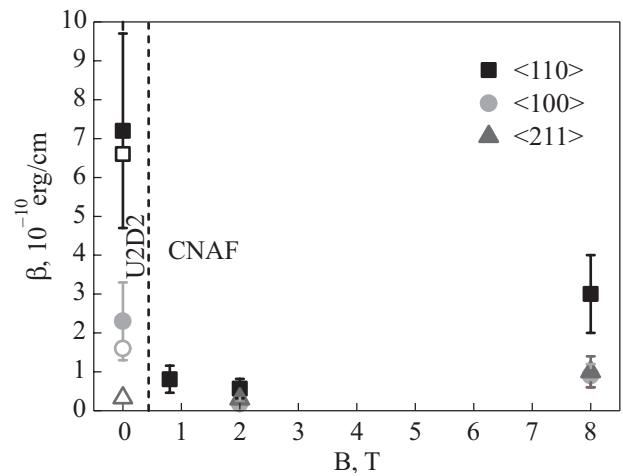


Fig. 15. Step energy of different facets below the Néel transition at different magnetic fields. Close symbols correspond with the step energies found by this work while the open symbols correspond with the work done by Tsepelin *et al.*[2].

leads to a linear behavior if a certain critical velocity is overcome (see Eq. (10)). In case that the step mobility would be low, it would mean that the step energy would be even lower. We can say that we have set an upper limit for the step energy of the $\langle 110 \rangle$, $\langle 100 \rangle$ and $\langle 211 \rangle$ facets. The calculated step energies are shown in Fig. 15.

Typically spiral growth occurs only for a driving force (overpressure) larger than a certain critical value as was observed in Ref. 2. In our analysis, all fits passed through the origin since the sensitivity of our pressure gauge was not good enough to determine this critical overpressure. If we could determine this overpressure and include it in the analysis, the step energies would decrease. Once again we can conclude that we have set an upper limit for the step energy.

The step energy of the $\langle 110 \rangle$ and $\langle 100 \rangle$ facets decreases by an order of magnitude at $B = 2$ T, while the $\langle 211 \rangle$ remains almost unaltered. At $B = 8$ T the $\langle 110 \rangle$ and $\langle 100 \rangle$ facets step energies have a value a bit lower than a factor of two compared with the value at zero magnetic field, while the $\langle 211 \rangle$ facet step energy increases by roughly a factor four its value. The $\langle 110 \rangle$ facet is the slowest at zero magnetic field but not anymore at higher magnetic fields, passing the $\langle 211 \rangle$ facet to be the slowest one.

We search for an effect of the magnetic orientation within the crystal with respect of the applied external magnetic field. The velocities of the same type of facets in a crystal, parallel and perpendicular to the field, were determined. The growth rate was the same for the same type of facets independently of its alignment with the magnetic field.

The ratio $\beta / \alpha d$ has been calculated for all the magnetic fields (see Table 5) in order to determine which limit is valid for the interaction between the liquid/solid interface with the crystal lattice.

Table 5. $\beta / \alpha d$ calculated for different facets at different magnetic fields.

B , T	Liquid \rightarrow Solid	$\langle 110 \rangle$	$\langle 100 \rangle$	$\langle 211 \rangle$
0	$B \rightarrow \text{U2D2}$	0.335	0.151	
0.8	$A \rightarrow \text{CNAF}$	0.038		
2	$A \rightarrow \text{CNAF}$	0.026	0.012	0.024
8	$A_1 \rightarrow \text{CNAF}$	0.139	0.059	0.081

It was found by Tsepelin *et al.* [2] that at zero magnetic field the interface couples strongly to the crystal lattice ($\beta / \alpha d \sim 1$) while it has been found experimentally that for ^4He $\beta / \alpha d \simeq 0.057$ [17]. It has been suggested [18] that in ^3He the coupling of the interface to the lattice would be even weaker than in ^4He [19] due to the larger zero-point motion of ^3He .

The results presented in this paper show that at zero magnetic field the interface couples strongly to the crystal lattice, but at $B = 0.8$ T, $B = 2$ T and $B = 8$ T the interface and the crystal lattice seem to be in the weak-coupling limit ($\beta / \alpha d \ll 1$).

Definitely more experiments are needed since there are too little experimental points to make a definite conclusion. The work presented in this paper shows indications that the phase transition from the U2D2 phase to the CNAF phase clearly affects the growth mechanisms of the crystals (Figs. 9 and 12).

It would be especially interesting to grow crystals slightly above and below the phase transition ($B = 450$ mT) where the liquid is in the superfluid B -phase. Then, from the same liquid phase, crystals could be grown into the two different magnetically ordered phases of the solid. As can be seen in the work by Ni *et al.* [16], the magnon velocity differs almost by a factor 2 in the transition from the U2D2 phase to the CNAF phase. If the magnon velocity turns out to be really the critical velocity (see Eq. (10)), the growth rates should also differ by a factor 2 below and above the transition.

Another interesting measurement would be to grow crystals slightly below 520 mT, where the liquid is in the superfluid B -phase and the solid is in the CNAF phase, and just above 520 mT, where the liquid is in the superfluid A -phase and the solid is in the CNAF phase. This would also give the possibility of studying the growth mechanisms starting from different initial liquid phases and to the same solid phase.

Another possible experiment would be to grow crystals at different magnetic fields in the CNAF phase and try to find out what the relation is between the step energy and the external magnetic field.

It would be also interesting to study the growth of crystals at high magnetic field both from the normal and superfluid phase and always below the Néel transition, since it seems to have some effect on the growth mechanisms (see Fig. 13,*d*). Difference in the thermal conductivity and diffusion properties in both liquid phases may affect the growth process.

Unfortunately the equilibrium shape of the crystals could not be studied in this paper. A new electrically actuated cold valve has been built [20]. In order to investigate the (slow) approach to the equilibrium shape of the crystal it is essential that no fluctuations in the volume of ^3He are present. These fluctuations are not caused directly because ^3He capillary is fully plugged, but indirectly through fluctuations in the ^4He pressure. With this valve closing off the ^4He filling line near the experimental cell, thermal and pressure fluctuations will be avoided and the crystal can go to its equilibrium shape without any external perturbation.

Acknowledgments

This work is part of the research programme of the Stichting voor Fundamenteel Onderzoek der Materie (FOM), which is financially supported by NWO.

Appendix A

The amount of solid, or the solid fraction, can be inferred from the volume of the cell [12]. For a compressional cell this volume can be obtained from the elasticity of the cell. In general, the relative volume change is related to the elasticity by

$$\frac{dv_3}{v_3} = \alpha d(P_3 - P_4), \quad (\text{A.1})$$

where P_3 is the pressure of the ^3He , P_4 the pressure of the ^4He , v_3 is the molar volume of the ^3He at the pressure P_3 , α is the elasticity of the cell, and dv_3 is the molar volume change due to a change $d(P_3 - P_4)$ in the pressure difference across the membrane. The elasticity can be obtained from a compression in the all-liquid phase:

$$\alpha = \frac{1}{v_3} \frac{dv_3}{d(P_3 - P_4)} = -\kappa_l \frac{dP_3}{d(P_3 - P_4)}, \quad (\text{A.2})$$

with κ_l the compressibility of liquid ^3He . Once α is known, a relation between P_3 , P_4 and x_s , the solid fraction, can be derived. Assume the liquid ^3He is being compressed by increasing the ^4He pressure (see Fig. 5), just until the melting curve is reached and solid is nucleated at the pressure P_{3m} , when the pressure P_{4m} is applied. Continuing the compression, the relative volume change along the melting curve is then given by

$$\begin{aligned} \frac{\Delta v_3}{v_l} &= \alpha \Delta(P_3 - P_4) = x_s \frac{v_s - v_l}{v_l} - (x_s \kappa_s + (1 - x_l) \kappa_l) \times \\ &\times (P_3 - P_{3m}) = x_s \frac{v_s - v_l}{v_l} - \kappa(P_3 - P_{3m}), \end{aligned} \quad (\text{A.3})$$

with $\Delta(P_3 - P_4) = (P_3 - P_4) - (P_{3m} - P_{4m})$ the change in $(P_3 - P_4)$ from the point of nucleation, v_l (v_s) the liquid (solid) molar volume at the pressure P_3 , and $\kappa \simeq \kappa_l \simeq \kappa_s$ the compressibility of liquid/solid ^3He at the melting pressure. Thus the solid fraction is given by

$$x_s = \frac{v_l}{v_s - v_l} [(\alpha + \kappa)(P_3 - P_{3m}) - \alpha(P_4 - P_{4m})]. \quad (\text{A.4})$$

1. V. Tsepelin, H. Alles, A. Babkin, J.P.H. Härme, R. Jochemsen, and A.Y. Parshin, *Phys. Rev. Lett.* **86**, 1042 (2001).
2. V. Tsepelin, H. Alles, A. Babkin, R. Jochemsen, A.Y. Parshin, and I.A. Todoshchenko, *Phys. Rev. Lett.* **88**, 045302 (2002).
3. D. Vollhardt and P. Wölfle, *The Superfluid Phases of Helium ^3He* , Taylor & Francis (1990).
4. S. Balibar, H. Alles, and A.Y. Parshin, *Rev. Mod. Phys.* **77**, 317 (2005).
5. F. Graner, S. Balibar, and E. Rolley, *J. Low Temp. Phys.* **75**, 69 (1989).
6. H.R. Akimoto, R. van Rooijen, A. Marchenkov, R. Jochemsen, and G. Frossati, *Physica* **B255**, 19 (2000).
7. V. Tsepelin, H. Alles, A. Babkin, R. Jochemsen, A.Y. Parshin, and I.A. Todoshchenko, *J. Low Temp. Phys.* **129**, 489 (2002).
8. A. Marchenkov, *Ph.D. Thesis*, Leiden University, unpublished (1997).
9. R. van Rooijen, A. Marchenkov, H. Akimoto, O. Andreeva, P. van der Haar, R. Jochemsen, and G. Frossati, *J. Low Temp. Phys.* **124**, 497 (2001).
10. R. Blaauwgeers, J. Bueno, D. Kleinhans, S. Leerink and R. Jochemsen, *J. Low Temp. Phys.* **134**, 393 (2004).
11. D.M.T. Dekker, R. Wagner, R. Blaauwgeers, J. Bueno, and R. Jochemsen, *J. Low Temp. Phys.* **139**, 509 (2005).
12. G. Vermeulen, *Ph.D. Thesis*, Leiden University (1986); see also the Appendix of this Paper.
13. R. Wagner, S.C. Steel, O. Andreeva, R. Jochemsen, and G. Frossati, *Phys. Rev. Lett.* **76**, 263 (1996).
14. V. Tsepelin, H. Alles, A. Babkin, J.P.H. Härme, R. Jochemsen, A.Y. Parshin, and G. Tvalashvili, *J. Low Temp. Phys.* **121**, 695 (2000).
15. H. Fukuyama, K. Yawata, T. Momoi, H. Ikegami, and H. Ishimoto, *arXiv:cond-mat/0505177* (2005).
16. W. Ni, J.S. Xia, and E.D. Adams, *Phys. Rev.* **B50**, 336 (1994).
17. E. Rolley, S. Balibar, F. Gallet, F. Graner, and C. Guthmann, *Europhys. Lett.* **8**, 523 (1989).
18. S. Balibar, C. Guthmann, and E. Rolley, *J. Phys. I France* **3**, 1475 (1993).
19. J.C. Heyraud, and J.J. Métois, *J. Cryst. Growth* **82**, 269 (1987).
20. J. Bueno, R. Blaauwgeers, R. Partapsing, I. Taminiau, and R. Jochemsen, *Rev. Sci. Instr.* **77**, 086103 (2006).